Journal of Colloid and Interface Science **236,** 305–317 (2001)
doi:10.1006/jcis.2000.7414, available online at http://www.idealibrary.com on IDEAL®

# Shape Factor Correlations of Hydraulic Conductance in Noncircular Capillaries

## II. Two-Phase Creeping Flow

T. W. Patzek[1] and J. G. Kristensen[2]

*Department of Civil and Environmental Engineering, 591 Evans Hall, University of California, Berkeley, CA 94720*

Received December 28, 2000; accepted December 29, 2000

**In Part I of this paper, we introduced the Mason–Morrow shape factor and the corner half-angles to capture the part of geometry of angular capillaries essential in pore network calculations of single- and two-phase flow in drainage and imbibition. We then used this shape factor to obtain simple expressions for the hydraulic conductance in single-phase flow through triangular, rectangular, and oval capillaries. In Part II, we study two-phase fluid flow along angular capillaries. The nonwetting fluid occupies the central part of the capillary, whereas the wetting liquid fills the corners. First, we verify the numerical solution obtained by Ransohoff–Radke for concave corner menisci by using a high-resolution finite element method with zero and infinite surface shear viscosity. We present new numerical results for corner flow domains bounded by convex menisci, i.e., for pinned contact lines and forced imbibition. We also present numerical solutions for two-phase flow with momentum transfer across the interface. We introduce a dimensionless hydraulic conductance of wetting fluid in the corners and correlate it with the corner filament shape factor, corner half-angle, and contact angle. By appropriate scaling, we obtain an accurate universal curve for flow conductance in the corners of an arbitrary angular capillary and for arbitrary contact angles. We give error estimates of the Ransohoff–Radke flow resistance factors, of the Zhou *et al*. analytical expressions for the resistance factors, and of our universal curves for the hydraulic conductance with no-slip and perfect-slip boundary conditions at the interface. Our expressions for the hydraulic conductance in corner flow of wetting liquid not only are valid for both concave and convex fluid interfaces but also are more accurate than any other published correlation.** 

*Key Words:* **corner flow; capillarity; shape factor; pore network; two-phase phase flow; correlation.**

### 1. INTRODUCTION

Earlier studies of liquid flow along angular capillaries involved mostly two phases. The nonwetting phase occupies the central part of the capillary, whereas the wetting phase fills the corners. Using a finite element method, Ransohoff and Radke (RR) (2) solved the creeping flow of a wetting liquid along the corners of a capillary occupied predominantly by a nonwetting gas phase. They investigated the effects of pore geometry (corner half-angle and corner rounding), contact angle, and surface shear viscosity. Their solution was tabulated in terms of a dimensionless resistance factor defined as

$$\chi_{\mathrm{RR}} = \frac{r^2(-\nabla p)}{\mu\langle v\rangle}, \qquad [2.1]$$

where $\nabla p$ is the pressure gradient driving the liquid flow in the corner, $r$ is the radius of curvature of the corner arc meniscus, and $\langle v\rangle$ is the average liquid velocity in the corner. The RR resistance factor is independent of the absolute size of the corner for a given geometry, but it has an unpleasant property of becoming infinite for a flat meniscus.

More recently, Zhou *et al*. (3) presented an approximate analytical solution for liquid flow in a noncircular capillary. Their solution predicts liquid flow rates for both two-phase and three-phase drainage. This solution is superior to other expressions in the literature based on the hydraulic radius and on the thin-film flow approximation, but it is not nearly as accurate as the correlations proposed here.

Creeping flow of three immiscible fluid phases in angular pores involves intermediate oil filaments sandwiched between water in the pore corners and gas in the pore center. The geometry of such a flow and oil filament stability have been described by Dong *et al*. (4). The hydraulic conductances in three-phase flow will be discussed in another paper.

In this paper, we derive accurate and simple correlations for the hydraulic conductance of corner filaments bounded by concave and convex interfaces that are rigid or allow perfect slip. Thus, our results are useful in predicting relative permeabilities not only in drainage and spontaneous imbibition with contact line pinning but also in forced imbibition with extreme hysteresis of contact angle.

[1] To whom correspondence should be addressed. E-mail: patzek@patzek.berkeley.edu. Tel: 510-643-5834.

[2] JGK has completed a master's thesis project at U.C. Berkeley as an exchange student between the Technical University of Denmark and the University of California.



0021-9797/01 $35.00

## 2. TWO-PHASE CREEPING FLOW IN CAPILLARIES

When a nonwetting fluid is present in angular capillaries, it forms filaments along the corners of the capillaries (sometimes loosely and incorrectly referred to as "corner films") and is separated from the nonwetting fluid by translationally symmetric arc-menisci (AMs). Equation [1.12] in Part I (1) is now written for each fluid (wetting "w" and nonwetting "o"):

$$\nabla^2 v_j + \frac{\Xi_j}{\mu_j} = 0, \quad \forall (x_1, x_2) \in \Omega_j,$$

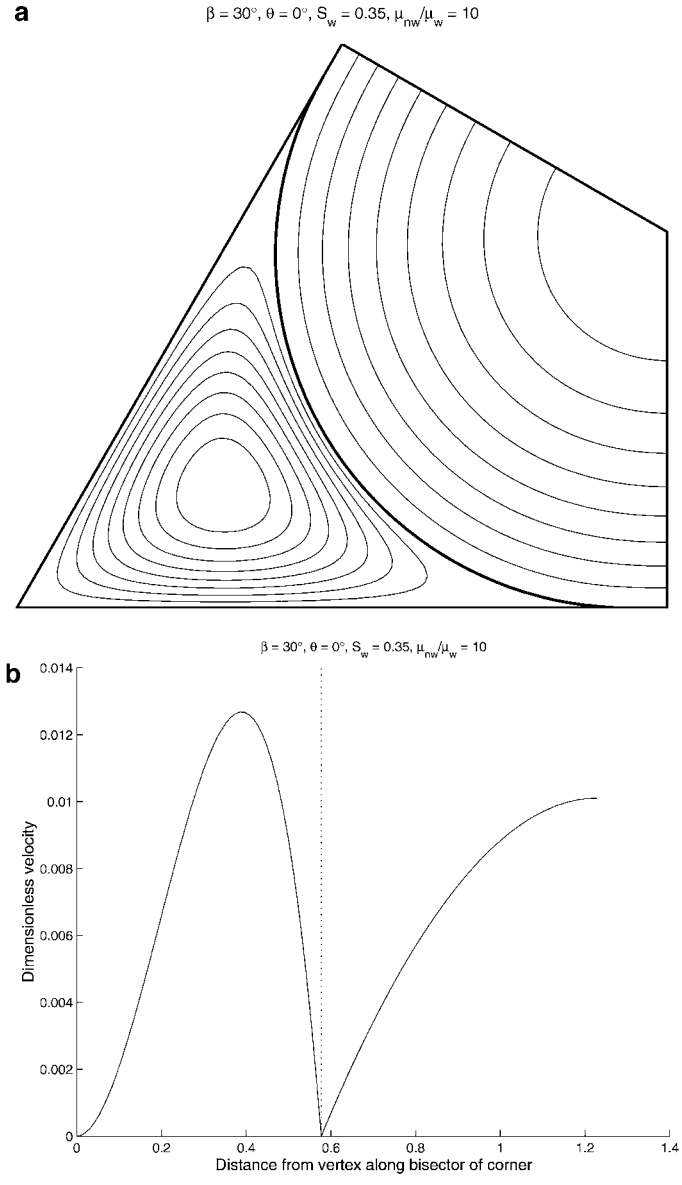


**FIG. 1.** Velocity distributions for the no-slip case. The corner half-angle is 30°, the contact angle is 0°, the wetting phase saturation is 0.35, and the nonwetting–wetting fluid viscosity ratio is 10: (a), velocity contours; (b), velocity profiles along the bisector of the corner angle, with the meniscus position highlighted by the vertical line.

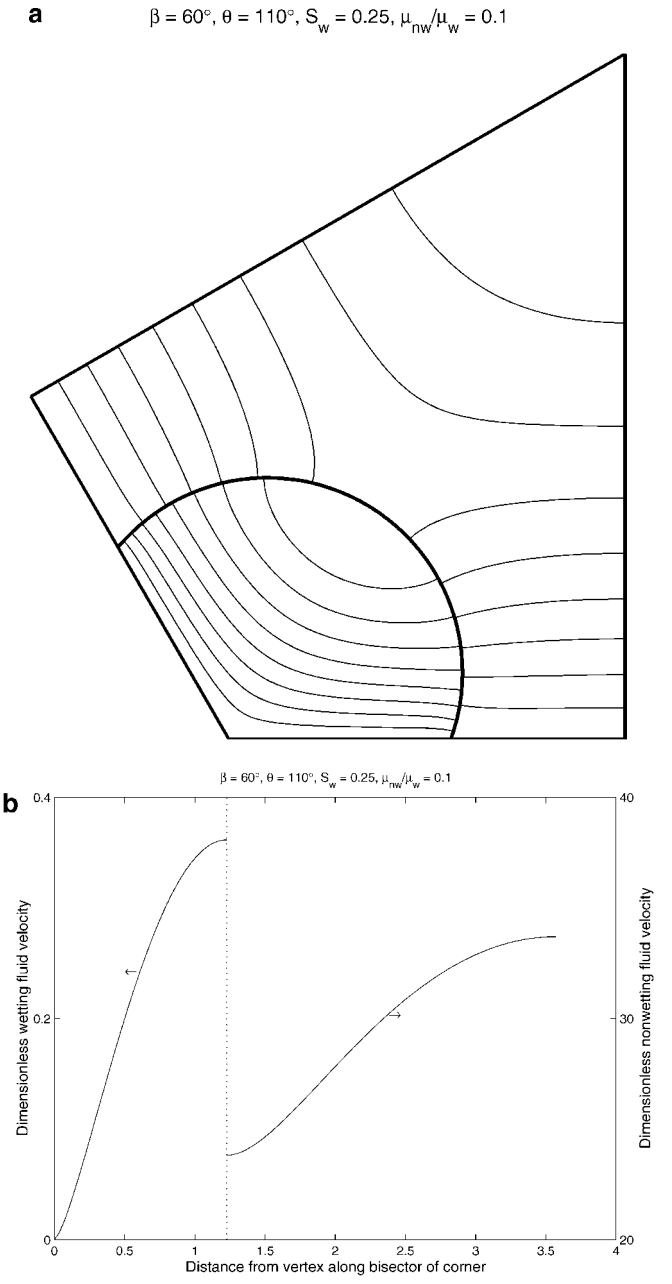


**FIG. 2.** Velocity distributions for the perfect-slip case. The corner half-angle is 60°, the contact angle is 110°, the wetting phase saturation is 0.25, and the nonwetting–wetting fluid viscosity ratio is 0.1: (a), velocity contours; (b), velocity profiles along the bisector of the corner angle, with the meniscus position highlighted by the vertical line.

$$\Xi_j = \left( \frac{\Delta p_j}{L} + \rho_j f_3 \right), \quad j = w, o. \qquad [2.2]$$

We assume that the bulk viscosities of the two fluids are constant, the interfacial tension is constant, and the buoyancy force is negligible in the duct; i.e., the Bond number is much less than one. With these assumptions the corner water filaments remain translationally symmetric and Eqs. [2.2] hold.

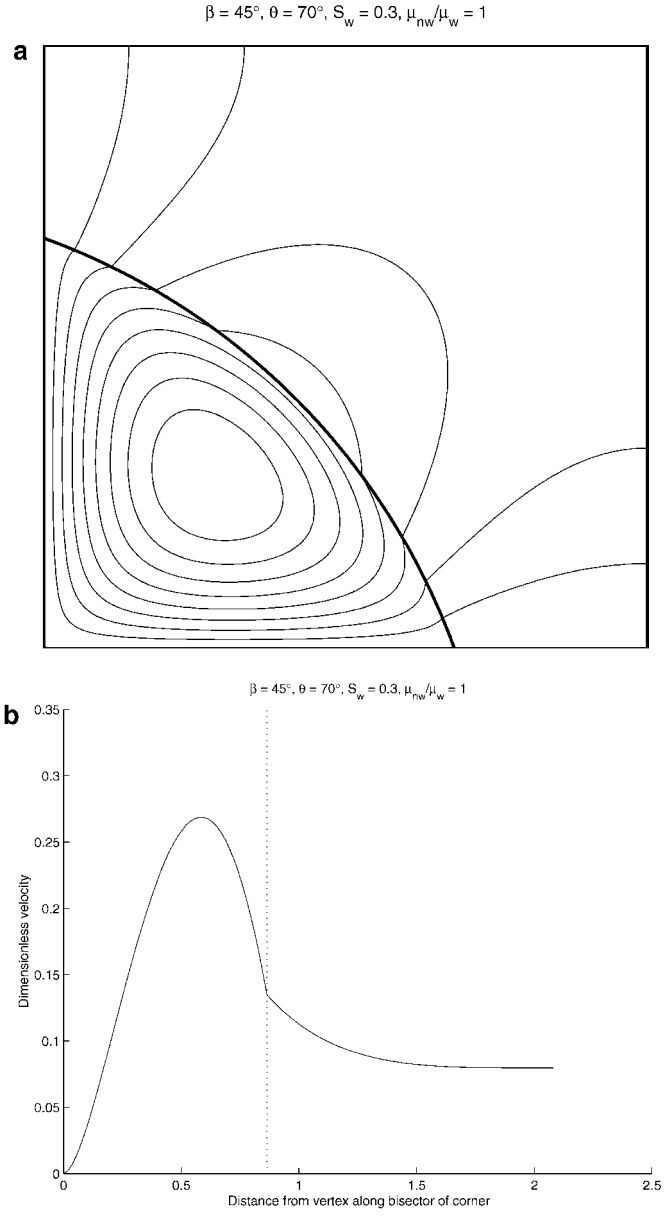


**FIG. 3.** Velocity distributions with continuity of velocity and shear stress across the interface. The corner half-angle is 45°, the contact angle is 70°, the wetting phase saturation is 0.30, and the nonwetting–wetting fluid viscosity ratio is 1: (a), velocity contours; (b), velocity profiles along the bisector of the corner angle, with the meniscus position highlighted by the vertical line.

In this paper, we shall only consider a single corner of a polygonal tube; i.e., both fluids will have symmetric flow domains, $\Omega_j$, bound by the tube walls, $s$, symmetry lines, *sym*, and AM, $ow$:$\Gamma_j = \Gamma_{sj} \cup \Gamma_{sym,j} \cup \Gamma_{ow}$.

We shall scale the spatial coordinates with the meniscus–apex distance $b$, and the fluid velocities with the wetting fluid viscosity and the respective average gradients of the driving force:

$$\tilde{x}_i = x_i/b, \quad i = 1, 2, 3 \qquad [2.3]$$

$$\tilde{v}_j = \frac{1}{\chi_j} = \frac{v_j \mu_w}{b^2 \Xi_j}, \quad j = w, o.$$

Equation [2.2] then becomes

$$\begin{aligned} \tilde{\mu}_j \nabla^2 \tilde{v}_j + 1 &= 0, \quad j = w, o \\ \tilde{\mu}_w &= 1, \quad \tilde{\mu}_o = \mu_o/\mu_w. \end{aligned} \qquad [2.4]$$

Note that $\chi_j$, the hydraulic resistance factor for fluid $j$, is

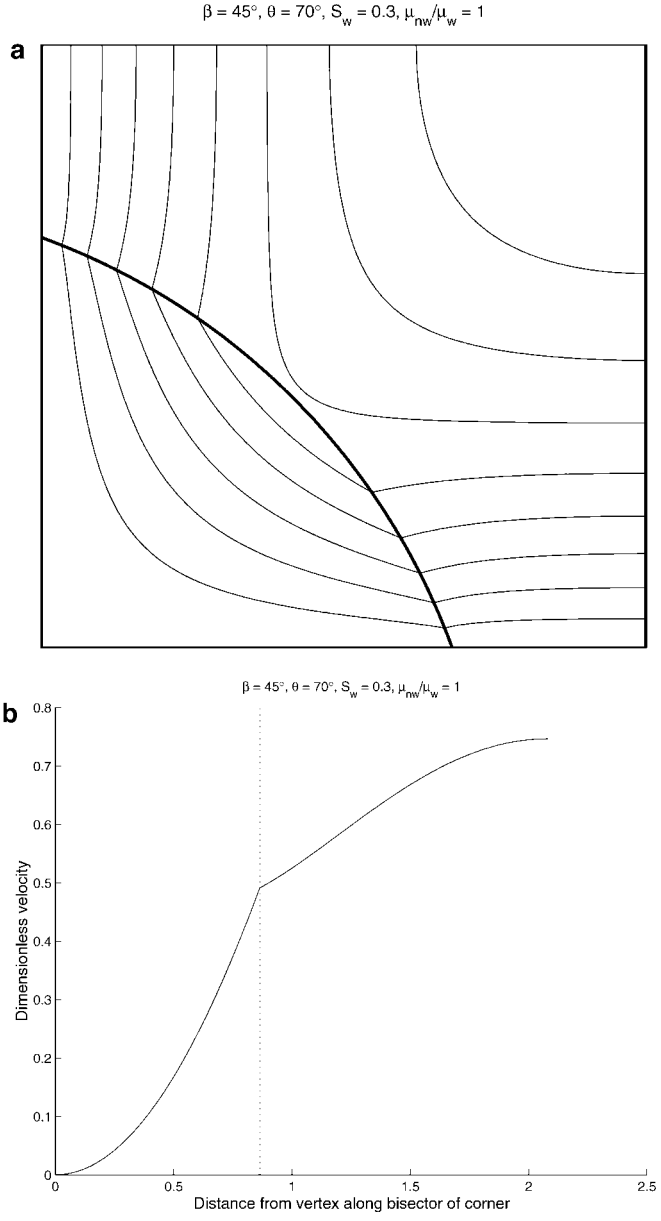


**FIG. 4.** Velocity distributions with continuity of velocity and shear stress across the interface. The corner half-angle is 45°, the contact angle is 70°, the wetting phase saturation is 0.30, and the nonwetting–wetting fluid viscosity ratio is 1: (a), velocity contours; (b), velocity profiles along the bisector of the corner angle, with the meniscus position highlighted by the vertical line.

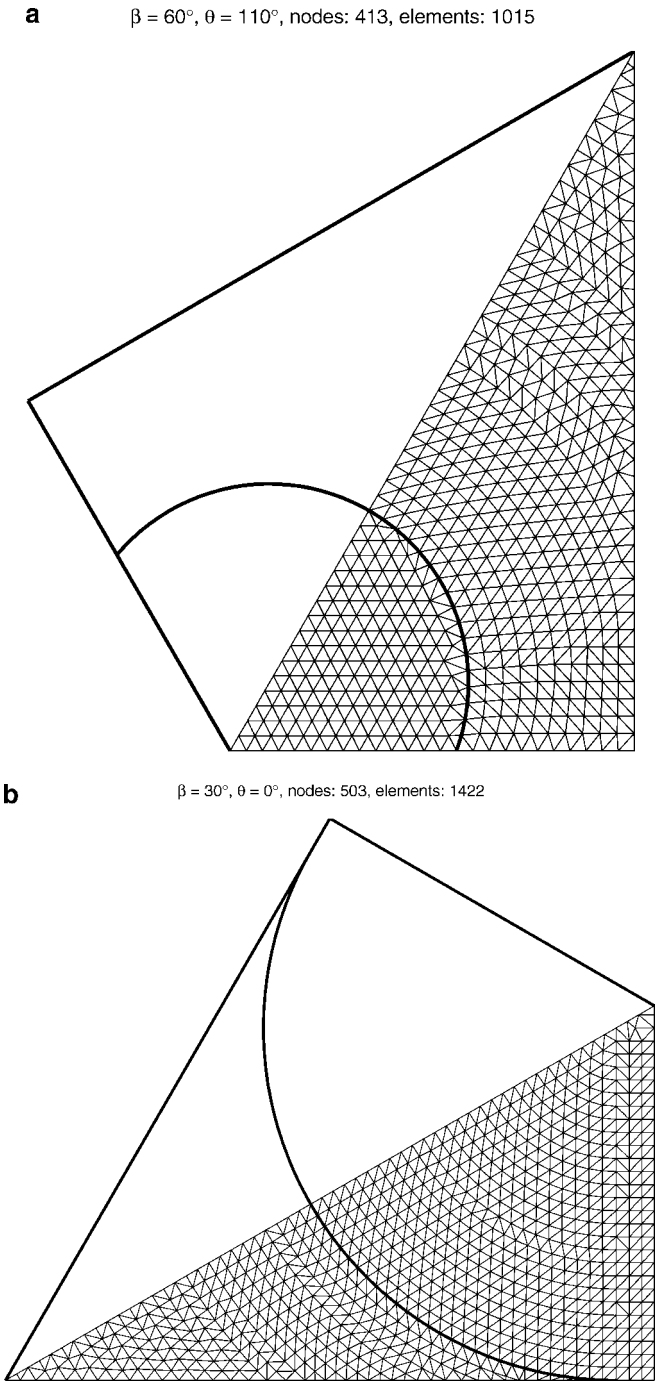


**FIG. 5.** Optimized finite element meshes for the corner half-angle of 60° and contact angle of 110° (a), and 30° and 0°, respectively, (b).

the inverse of the dimensionless average velocity defined in Eq. [2.3]. A somewhat different definition of the hydraulic resistance factor has been proposed by Ransohoff and Radke (2), who used the meniscus radius of curvature, $r_p$, instead of the inscribed circle radius as in Eq. [1.15] or the meniscus–apex distance as in Eq. [2.3]. In Ransohoff and Radke's formulation, the resistance factor goes to infinity as the meniscus becomes flat, but the ratio $\chi / r_p^2$ remains finite. Their scaling causes a severe loss of precision in the numerically determined resistance factors for almost flat menisci and makes it quite difficult to correlate the hydraulic conductance with capillary geometry and fluid properties.

In all cases, we shall impose a no-slip boundary condition along the duct walls and a no flow condition across the lines of symmetry:

$$\begin{aligned} \tilde{v}_j &= 0, \quad \text{on } \Gamma_{sj} \\ \nabla \tilde{v}_j \cdot \vec{n}_j &= 0, \quad \text{on } \Gamma_{sym,j} \end{aligned} \qquad [2.5]$$

where $\vec{n}_j$ is the unit outward normal vector along $\Gamma_j$.

We shall consider three different boundary conditions along the AM. The first boundary condition requires infinite surface shear viscosity of the interface, which becomes a

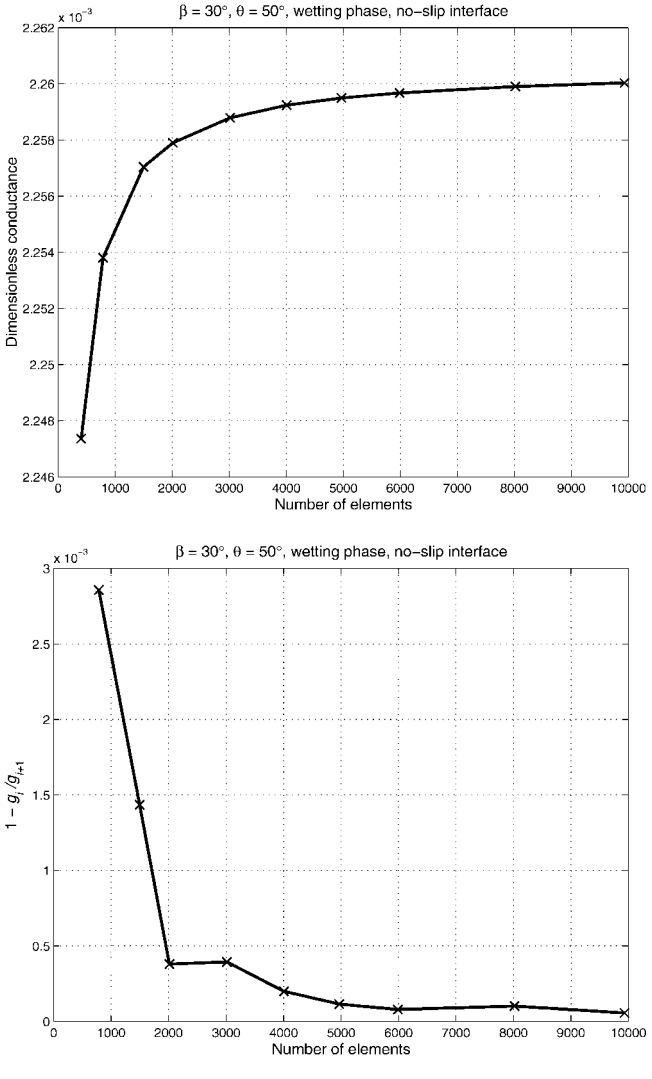


**FIG. 6.** Convergence of the FE solution for the wetting fluid hydraulic conductance in the perfectly rigid interface case.

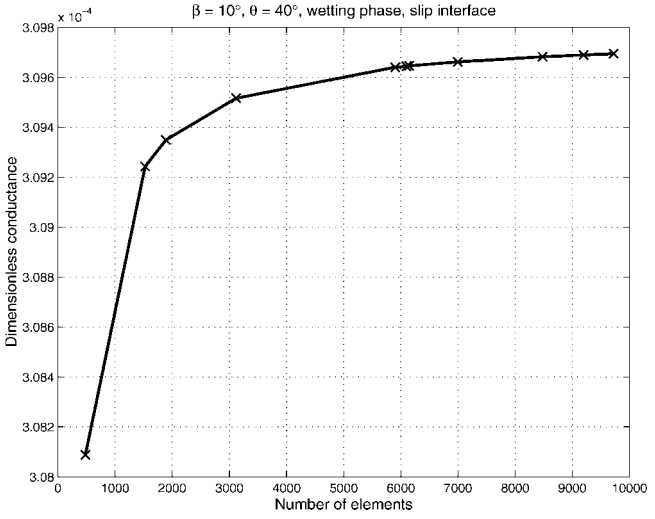


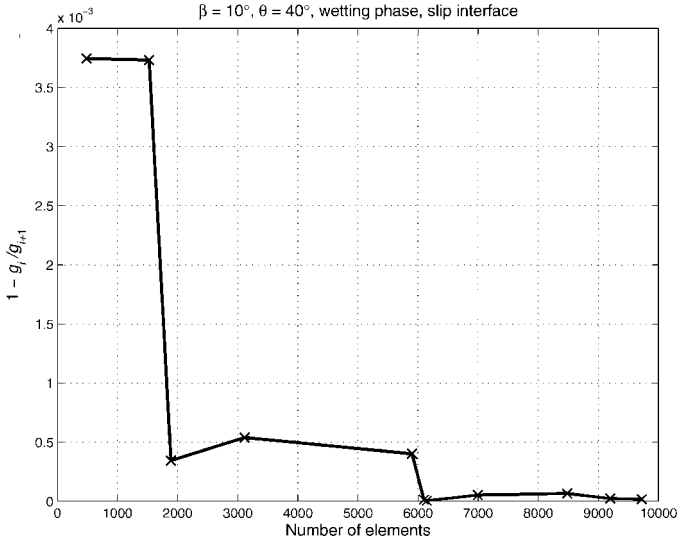


**FIG. 7.** Convergence of the FE solution for the wetting fluid hydraulic conductance in the perfect-slip interface case.

surfactant-laden rigid wall with a no-slip condition (Fig. 1):

$$\tilde{v}_j = 0, \quad \text{on } \Gamma_{ow}. \qquad [2.6]$$

**TABLE 1**
**The Hydraulic Resistance Factors with Perfect Slip at the Meniscus and Zero Contact-Angle[a]**

| $\beta$ | 10° | 15° | 30° | 36° | 45° | 60° | 72° |
|---|---|---|---|---|---|---|---|
| $\chi_{RR}$ | 9.981 | 12.95 | 31.07 | 46.67 | 93.93 | 443.0 | 3185 |
| $\chi_{r_c}$ | 9.627 | 12.47 | 30.10 | 45.30 | 91.39 | 432.2 | 3113 |
| % Deviation | 3.55 | 3.71 | 3.12 | 2.94 | 2.70 | 2.44 | 2.26 |
| $\chi$ | 275.4 | 145.5 | 90.29 | 85.83 | 91.39 | 144.1 | 328.6 |

[a] $\chi_{RR}$ are the resistance factors reported by Ransohoff and Radke (2); $\chi_{r_c}$, are the resistance factors calculated here, but scaled with the meniscus radius of curvature; $\chi$ are the resistance factors scaled with the meniscus–apex distance; and % Deviation $= |\chi_{r_c}/\chi_{RR} - 1| \times 100\%$.

The second boundary condition describes a liquid–gas interface (Fig. 2), and the third describes two immiscible liquids separated by a clean interface (Figs. 3 and 4). In the former case, gas slips along the interface, and there is no momentum transfer across the AM:

$$\nabla\tilde{v}_j \cdot \vec{n}_j = 0, \quad j = w, o, \quad \forall(\tilde{x}_1, \tilde{x}_2) \in \Gamma_{ow}. \qquad [2.7]$$

In the latter case there is continuity in velocity and shear stress:

$$\nabla\tilde{v}_w \cdot \vec{n}_w = \tilde{\mu}\nabla\tilde{v}_o \cdot \vec{n}_o, \quad \forall(\tilde{x}_1, \tilde{x}_2) \in \Gamma_{ow}. \qquad [2.8]$$

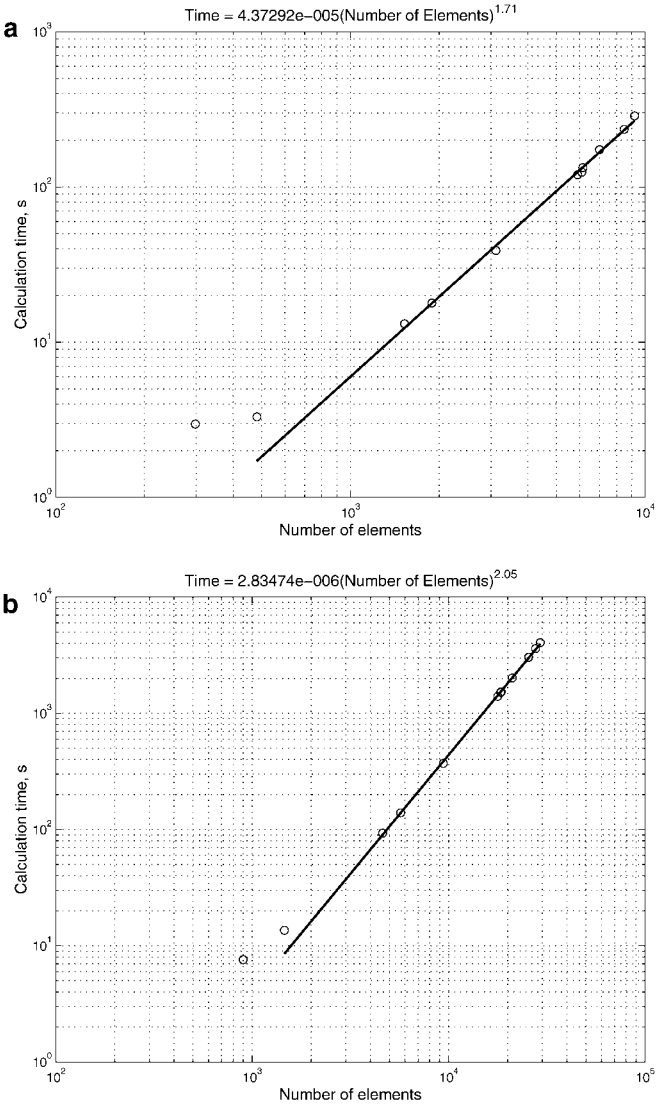


**FIG. 8.** (a) Calculation times for $\beta = 10°, \theta = 40°$, no-slip boundary condition, and only wetting fluid domain. (b) Calculation times for $\beta = 10°, \theta = 40°$, perfect-slip boundary condition, and both domains with $S_w = 0.25$.

**TABLE 2**
**Calculated Hydraulic Conductances of Wetting Fluid with No Slip at the Interface**

| $\downarrow \theta$ | $\beta = 10$ | $\beta = 15$ | $\beta = 30$ | $\beta = 36$ | $\beta = 45$ | $\beta = 60$ | $\beta = 72$ |
|---|---|---|---|---|---|---|---|
| 0 | 0.000155808 | 0.000319473 | 0.000591405 | 0.000564288 | 0.000434617 | 0.000477339 | 4.25907e-05 |
| 10 | 0.000174368 | 0.000378922 | 0.000850795 | 0.000888907 | 0.000804681 | 0.00101165 | 0.000222321 |
| 20 | 0.000191802 | 0.000437588 | 0.00114934 | 0.00128838 | 0.00131402 | 0.00182931 | 0.000649401 |
| 30 | 0.000208288 | 0.00049545 | 0.00148394 | 0.00176084 | 0.00197091 | 0.00298816 | 0.00143123 |
| 40 | 0.00022402 | 0.000552701 | 0.00185362 | 0.00230717 | 0.00278621 | 0.00456531 | 0.0026915 |
| 50 | 0.000239164 | 0.000609669 | 0.00225972 | 0.00293215 | 0.00377969 | 0.00666428 | 0.00458976 |
| 60 | 0.000253905 | 0.000666807 | 0.00270524 | 0.00364313 | 0.00497461 | 0.00943488 | 0.0073502 |
| 70 | 0.000268437 | 0.000724761 | 0.00319679 | 0.00445492 | 0.0064125 | 0.0131032 | 0.0113042 |
| 80 | 0.000282959 | 0.000784254 | 0.00374405 | 0.0053891 | 0.00815315 | 0.0180192 | 0.0169683 |
| 90 | 0.000297719 | 0.000846297 | 0.00436162 | 0.00647807 | 0.0102866 | 0.0247521 | 0.0251854 |
| 100 | 0.000312937 | 0.00091199 | 0.00507049 | 0.00777005 | 0.0129508 | 0.0342459 | 0.0374129 |
| 110 | 0.000328942 | 0.000982951 | 0.00590111 | 0.00933639 | 0.0163579 | 0.0481978 | |
| 120 | 0.000346156 | 0.00106136 | 0.00690075 | 0.0112905 | 0.0208584 | | |
| 130 | 0.00036513 | 0.00115033 | 0.00814316 | 0.0138159 | 0.0270501 | | |
| 140 | 0.000386675 | 0.00125455 | 0.00974994 | 0.0172259 | | | |
| 150 | 0.00041201 | 0.00138132 | 0.0119327 | | | | |
| 160 | 0.000443099 | 0.00154289 | | | | | |
| 170 | 0.00048327 | | | | | | |

The dimensionless velocities in Eq. [2.8] are scaled with respect to the driving pressure gradient in the fluid that drags the other. Because of the same scaling, no ratio of the respective gradients appears in Eq. [2.8].

The average dimensionless velocities are calculated as follows:

$$\langle \tilde{v}_j \rangle = \frac{1}{\tilde{A}_j} \int_{\Omega_j} \tilde{v}_j d\tilde{A}, \quad j = w, o. \qquad [2.9]$$

The conductances are calculated from Eq. [1.13] specified for each phase

$$Q_j = \int_{\Omega_j} v_j dA = \boldsymbol{g}_j \Xi_j = \frac{b^4}{\mu_w} \int_{\Omega_j} \tilde{v}_j d\tilde{A} = \frac{b^4}{\mu_w} \tilde{\boldsymbol{g}}_j,$$
$$j = w, o. \qquad [2.10]$$

## 3. FINITE ELEMENT MODEL

A standard Galerkin finite element code, e.g., Refs. (5, 6), with triangular elements and linear basis functions was written

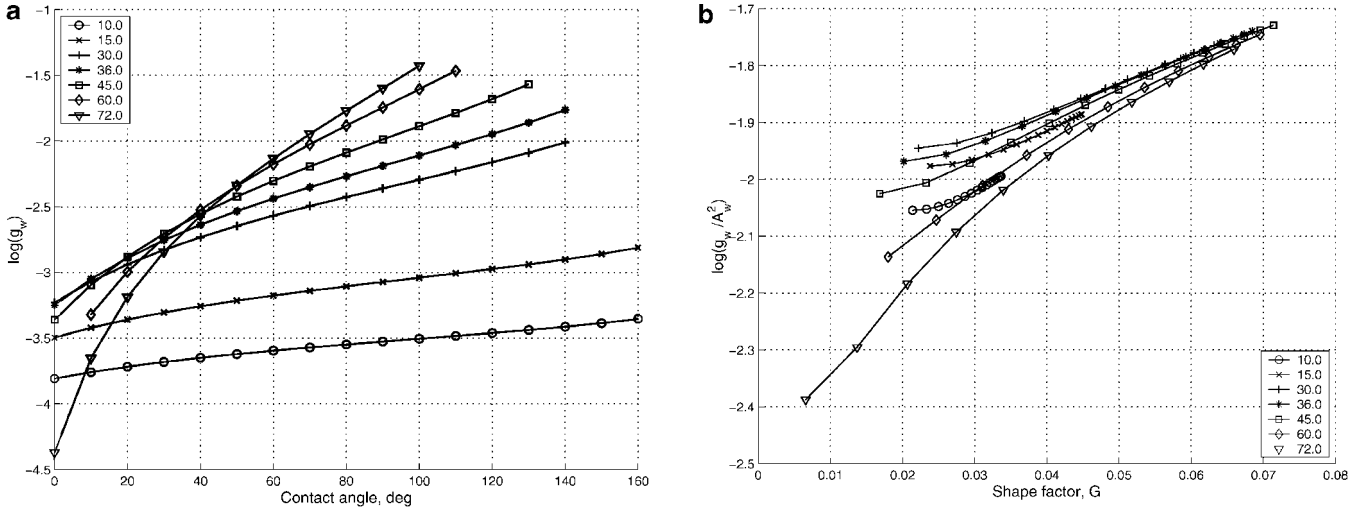


**FIG. 9.** (a) The logarithm of the dimensionless hydraulic conductance vs. contact angle. (b) The logarithm of the ratio of the dimensionless hydraulic conductance and the dimensionless corner filament area squared plotted vs. the filament shape factor. The half-angles of the corners are between 10° and 72°.

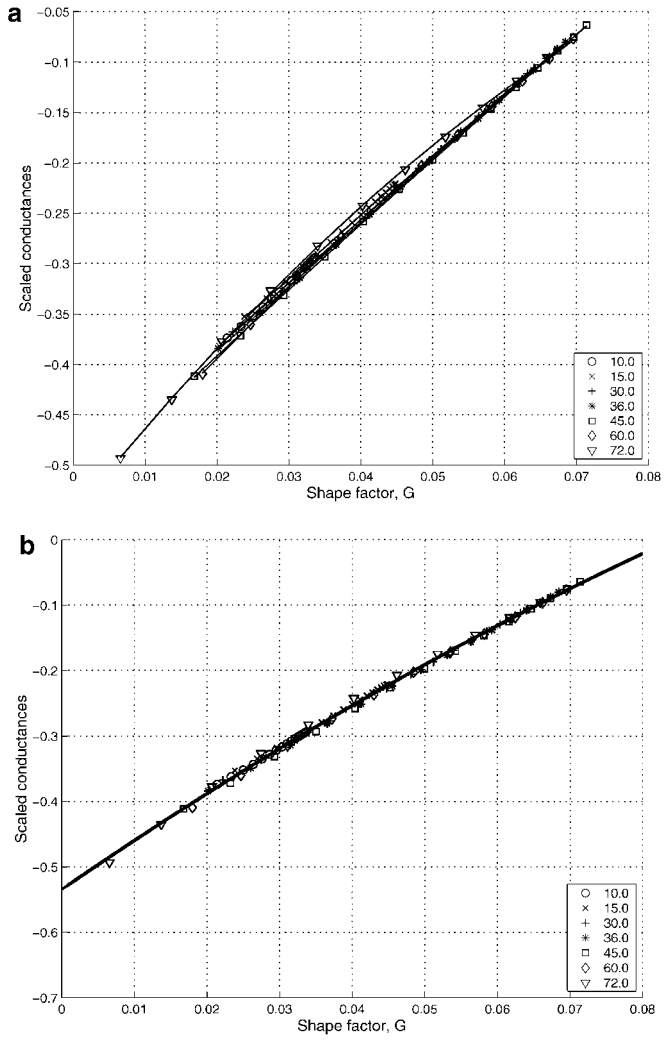


**FIG. 10.** The scaled hydraulic conductance approximations for each corner half-angle (a) and the single master curve (b) vs. the filament shape factor.

(7) and implemented in MATLAB (8). The only innovation is in the generation of triangular meshes that always follow the meniscus and domain shapes (Fig. 5). A custom MATLAB program, employing Delaunay triangulation, was written to achieve high accuracy and consistent precision with about the same number of elements for all corner half-angles, contact angles, and boundary conditions.

**TABLE 3**
**Quadratic Approximations [2.16] of Scaled Hydraulic Conductances [2.15] in No-Slip Case**

| $\beta,^\circ$ | $a_1$ | $a_2$ | $a_3$ |
|---|---|---|---|
| 10 | 44.7742 | 4.11225 | −0.482575 |
| 15 | 14.1251 | 5.35202 | −0.488549 |
| 30 | 0.467423 | 6.23521 | −0.506957 |
| 36 | −1.62722 | 6.46701 | −0.515126 |
| 45 | −5.2275 | 6.85371 | −0.526681 |
| 60 | −16.9201 | 7.89046 | −0.544937 |
| 72 | −30.726 | 8.8734 | −0.549388 |
| Master curve | −15.1794 | 7.6307 | −0.53448 |

### *3.1. Convergence*

As the number of elements increases, the solution will become more accurate until it reaches a computer-specific limit, beyond which the difference between two consecutive solutions is small and random. One way of testing convergence is to plot the calculated hydraulic conductances versus the corresponding number of finite elements. Another is to plot the relative difference between two consecutive solutions,

$$\left|\frac{\boldsymbol{g}_j^{N_2}-\boldsymbol{g}_j^{N_1}}{\boldsymbol{g}_j^{N_2}}\right| = \left|1-\frac{\boldsymbol{g}_j^{N_1}}{\boldsymbol{g}_j^{N_2}}\right|, \quad N_2 > N_1 = \text{number of elements}, \tag{2.11}$$

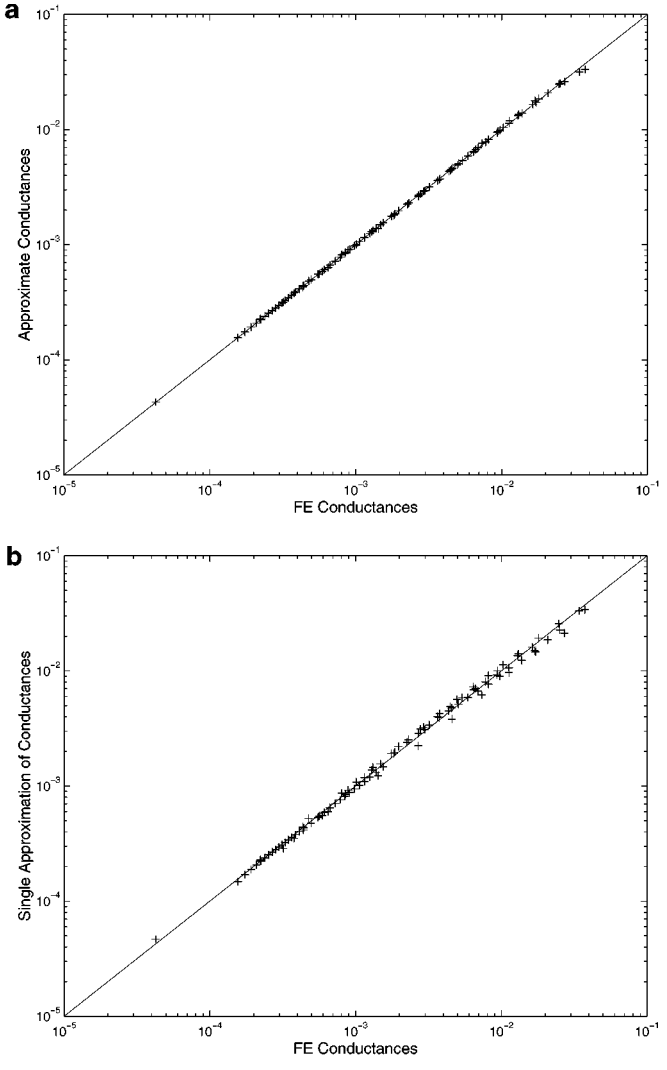


**FIG. 11.** Individual approximations for each corner half-angle (a) and a single approximation (b) for all corner half-angles versus the finite element results in the no-slip case.

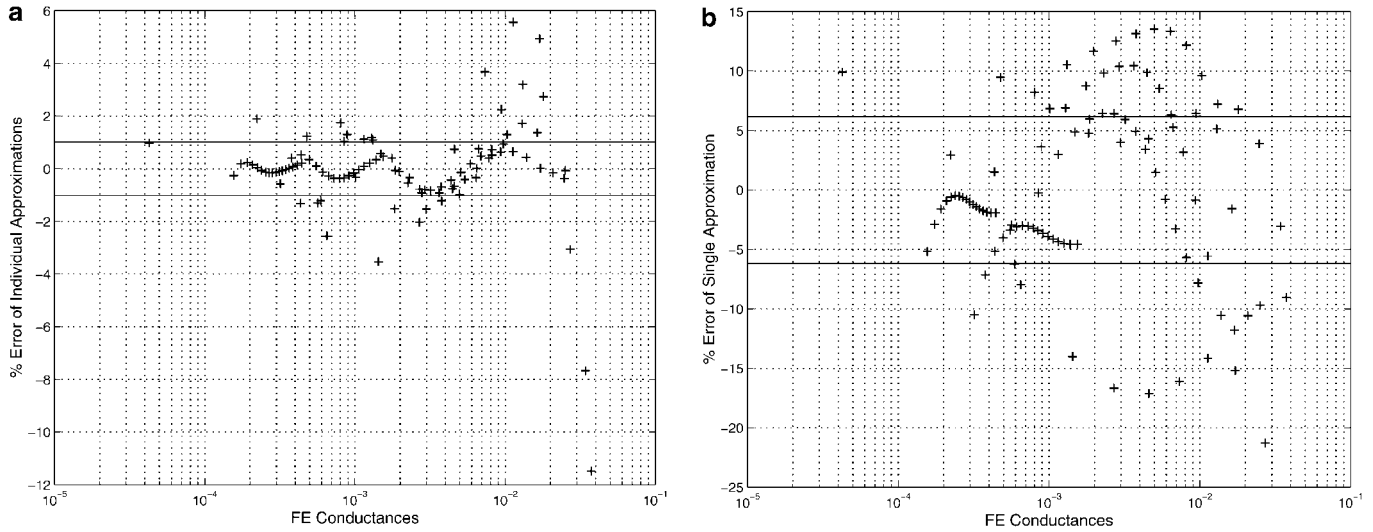


**FIG. 12.** The mean absolute error of the individual approximations (a) in the no-slip case is 1%, while that of the single approximation (b) is 6.2%.

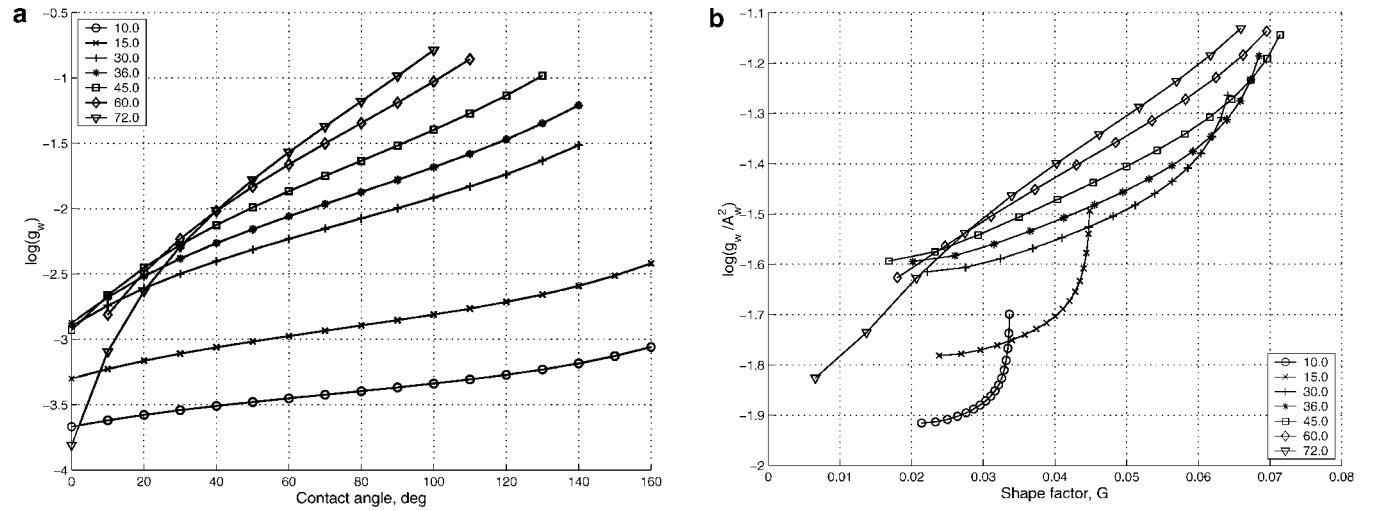


**FIG. 13.** (a) The logarithm of the dimensionless hydraulic conductance in the perfect-slip case vs. contact angle. (b) The logarithm of the ratio of the dimensionless hydraulic conductance and the dimensionless corner filament area squared plotted vs. the filament shape factor. The half-angles of the corners are between 10° and 72°.

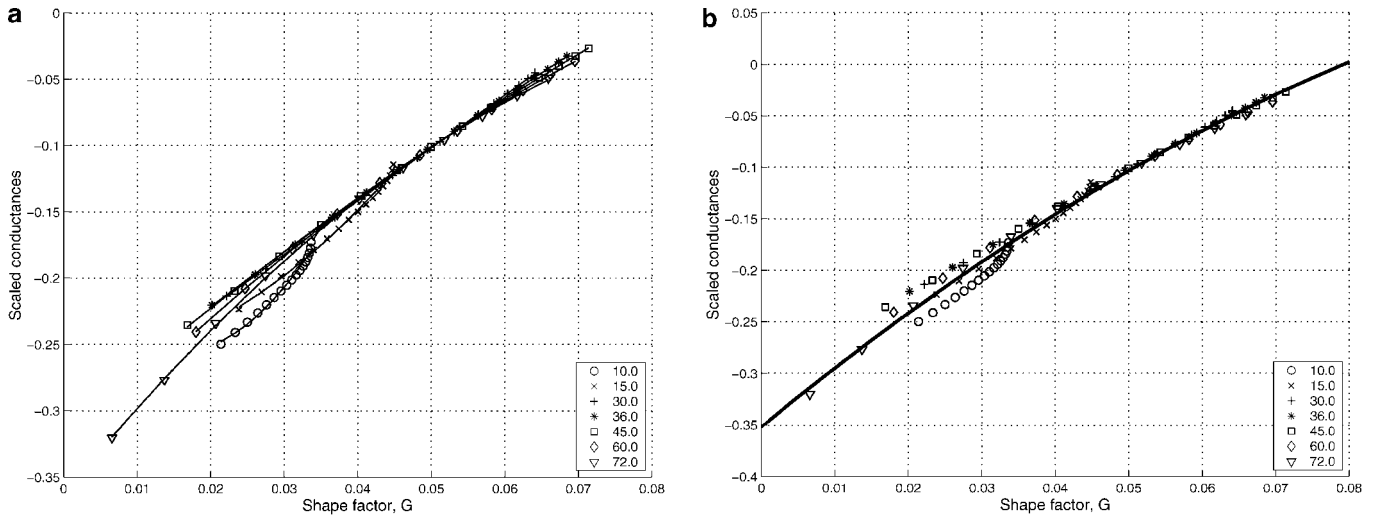


**FIG. 14.** The scaled hydraulic conductance approximations for each corner half-angle (a) and the single master curve (b) vs. the filament shape factor.

**TABLE 4**
**Calculated Hydraulic Conductances of Wetting Fluid with Perfect Slip at the Interface**

| $\downarrow \theta$ | $\beta = 10$ | $\beta = 15$ | $\beta = 30$ | $\beta = 36$ | $\beta = 45$ | $\beta = 60$ | $\beta = 72$ |
|---|---|---|---|---|---|---|---|
| 0 | 0.000214652 | 0.000500772 | 0.00126421 | 0.00133431 | 0.00117405 | 0.00154473 | 0.0001551 |
| 10 | 0.000240239 | 0.000593971 | 0.00181791 | 0.00210033 | 0.00217106 | 0.00325816 | 0.000806533 |
| 20 | 0.000264354 | 0.000686101 | 0.00245387 | 0.00303992 | 0.00353619 | 0.00586994 | 0.00233999 |
| 30 | 0.000287351 | 0.000777557 | 0.00316825 | 0.00415228 | 0.00529511 | 0.00959399 | 0.00513610 |
| 40 | 0.000309646 | 0.000869341 | 0.00396545 | 0.00544978 | 0.00749477 | 0.014745 | 0.00966772 |
| 50 | 0.000331683 | 0.000962891 | 0.00485841 | 0.00696111 | 0.0102187 | 0.0218057 | 0.0166134 |
| 60 | 0.000353963 | 0.00106016 | 0.00587008 | 0.00873522 | 0.0135973 | 0.0315369 | 0.0270284 |
| 70 | 0.000377045 | 0.00116360 | 0.00703615 | 0.0108498 | 0.0178391 | 0.0451727 | 0.0426319 |
| 80 | 0.000401592 | 0.00127636 | 0.00840959 | 0.0134224 | 0.0232668 | 0.0647756 | 0.0663468 |
| 90 | 0.000428415 | 0.00140261 | 0.0100691 | 0.0166323 | 0.0303885 | 0.0939383 | 0.103370 |
| 100 | 0.000458593 | 0.00154811 | 0.0121339 | 0.0207582 | 0.0400262 | 0.139229 | 0.163441 |
| 110 | 0.000493595 | 0.00172107 | 0.0147891 | 0.0262470 | 0.0535577 | 0.213424 | |
| 120 | 0.000535530 | 0.00193369 | 0.0183348 | 0.0338452 | 0.0734054 | | |
| 130 | 0.000587585 | 0.00220495 | 0.0232775 | 0.0448594 | 0.104066 | | |
| 140 | 0.000654802 | 0.00256571 | 0.0305199 | 0.0617122 | | | |
| 150 | 0.000745484 | 0.00306844 | 0.0417729 | | | | |
| 160 | 0.000874266 | 0.00380897 | | | | | |
| 170 | 0.00106830 | | | | | | |

versus the number of elements. Figures 6 and 7 show two examples of this approach for different corner angles, contact angles, and boundary conditions. As one can see, with about 6000 finite elements representing *both* flow domains, our solutions converge to machine precision: 64 bits in our case. This observation has been confirmed in every calculation presented here. In contrast, the finite element solutions of Ransohoff and Radke (2) had been obtained with fewer[3] elements and were not quite converged (Table 1). The discrepancies between both sets of results are up to 4%.

In the case of continuity of shear stress across the interface, the flows of both fluids are coupled (9). Neglecting gravity, we have

$$\begin{aligned} Q_w &= -\boldsymbol{g}_w \nabla p_w - \boldsymbol{g}_w^o \nabla p_0, \\ Q_o &= -\boldsymbol{g}_o \nabla p_o - \boldsymbol{g}_o^w \nabla p_w. \end{aligned} \qquad [2.12]$$

Of course, the Onsager reciprocity requires that coupling terms be $\boldsymbol{g}_w^o = \boldsymbol{g}_o^w$. To check the implementation of boundary condition [2.8], we solve the FE model twice. First, we set the pressure gradient in the wetting phase to 1 and that in the nonwetting phase to 0. Second, we do the opposite. We then compare the calculated coupling terms. The largest difference has been $1 \times 10^{-14}$. The main reason for such a high accuracy is our grid, which has nodes precisely along the meniscus.

### 3.2. Calculation Times

Because the finite element mesh is adjusted to fit the meniscus shape and flow domain geometry, the computation time scales roughly as the number of elements to the power 1.75 and 2, respectively, for one- and two-domain calculations (Fig. 8). Still, a 6500-element calculation takes about two minutes on a 330 MHz Pentium Pro computer running MATLAB 5.2.1.1240.[4] This time includes the generation of all plots and their encapsulated PostScript images.

## 4. RESULTS

### 4.1. Infinite Surface Shear Viscosity

We assume that each AM surface is laden with surfactants and rigid, resulting in the no-slip boundary conditions along the pore walls and the meniscus (see Table 2). The dimensionless corner flow conductances have been calculated for a variety of corner half-angles and contact angles (Fig. 9).

With $b = 1$, the dimensionless flow cross-sectional area and shape factor of the corner filament are calculated as follows:

$$\tilde{A}_w = \begin{cases} \sin\beta\cos\beta, & \text{if } \theta + \beta = \pi/2 \\ \left(\dfrac{\sin\beta}{\cos(\theta+\beta)}\right)^2 \left(\dfrac{\cos\theta\cos(\theta+\beta)}{\sin\beta} + \theta + \beta - \dfrac{\pi}{2}\right) \end{cases} \qquad [2.13]$$

otherwise

$$\tilde{G} = \begin{cases} \dfrac{\tilde{A}_w}{4(1+\sin\beta)^2}, & \text{if } \theta + \beta = \pi/2 \\ \dfrac{\tilde{A}_w}{4[1 - \sin\beta/\cos(\theta+\beta)(\theta+\beta-\pi/2)]^2}. \end{cases} \qquad [2.14]$$

[3] Dr. Ransohoff recalls using 400–600 elements in *single* flow domain calculations (e-mail, June 7, 1999).

[4] There was no speed gain in runs under MATLAB 5.3.1.29215A (R11.1).

**TABLE 5**
**Quadratic Approximations [2.16] of Scaled Hydraulic Conductances [2.15] in Perfect-Slip Case**

| $\beta,^\circ$ | $a_1$ | $a_2$ | $a_3$ |
|---|---|---|---|
| 10 | 224.885 | −6.80214 | −0.205123 |
| 15 | 68.3560 | 0.15000 | −0.264133 |
| 30 | −1.52067 | 4.13661 | −0.304756 |
| 36 | −6.07127 | 4.43528 | −0.307906 |
| 45 | −10.7395 | 4.79784 | −0.314243 |
| 60 | −19.9801 | 5.69843 | −0.336266 |
| 72 | −31.5714 | 6.82525 | −0.363203 |
| Master curve | −18.2066 | 5.88287 | −0.351809 |

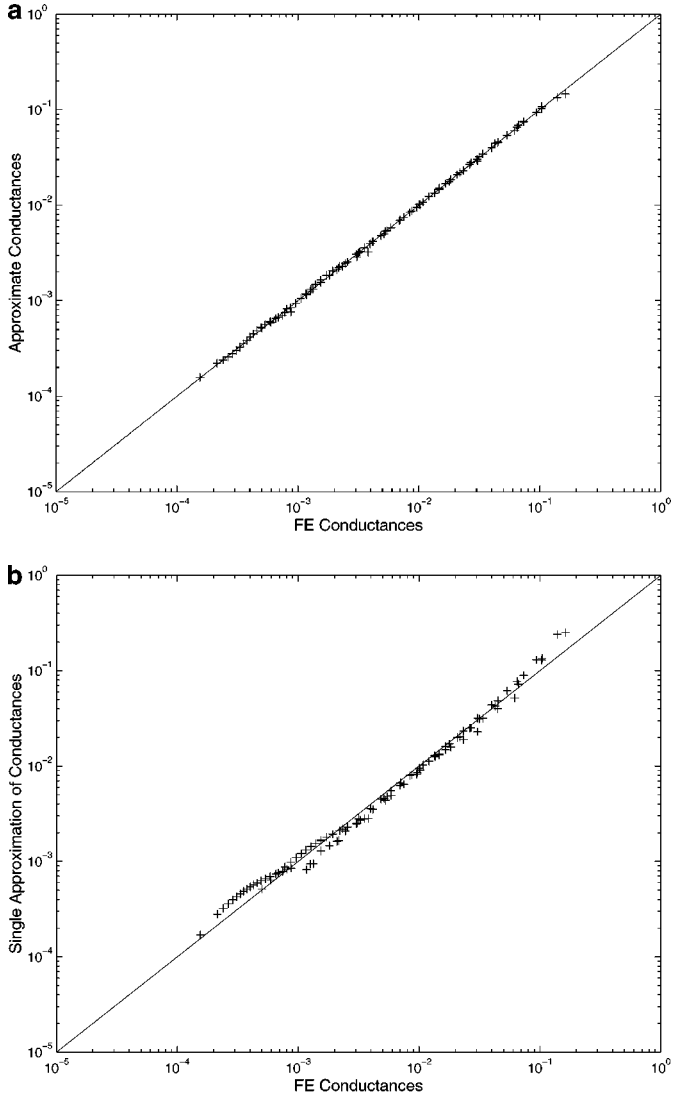


**FIG. 15.** Individual approximations for each corner half-angle (a) and a single approximation (b) for all corner half-angles versus the finite element results in the perfect-slip case.

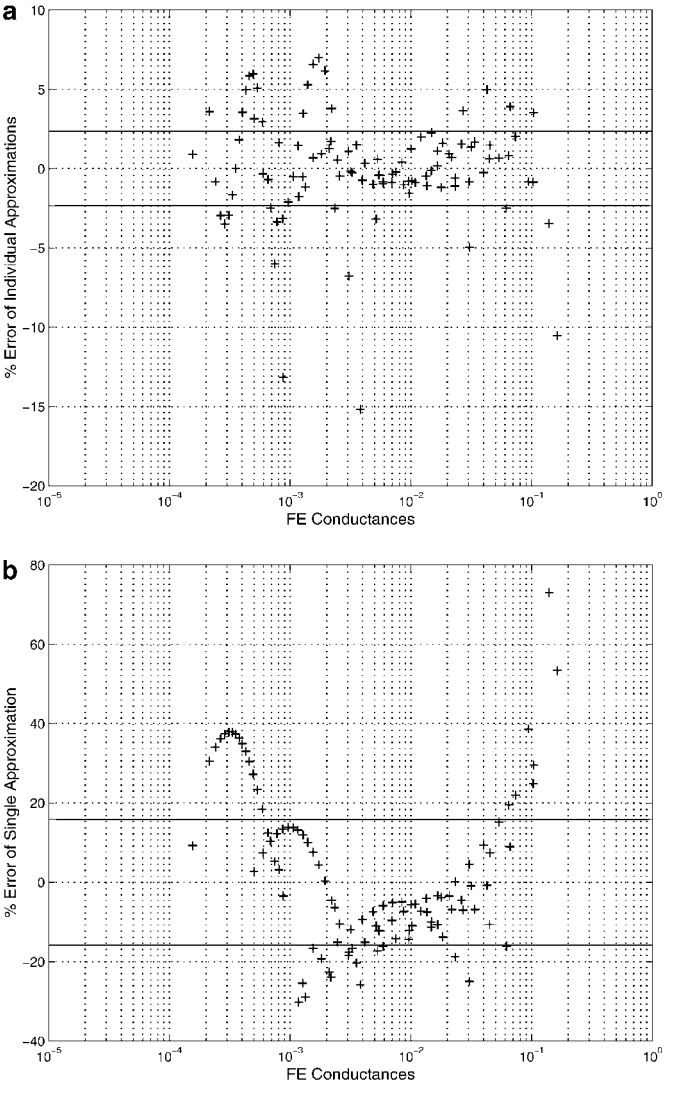


**FIG. 16.** The mean absolute error of the individual approximations (a) in the perfect-slip case is 2.2%, while that of the single approximation (b) is 15.9%.

We propose to scale the dimensionless hydraulic conductance of the corner liquid filaments as follows:

$$\tilde{g}_w = \ln\left(\frac{\tilde{g}_w}{\tilde{A}_w^2}\right)\left(\frac{1}{4\pi} - \tilde{G}\right)^{e_1} \cos^{e_2}\left(\beta - \frac{\pi}{6}\right) - 0.02\sin\left(\beta - \frac{\pi}{6}\right). \quad [2.15]$$

In the no-slip case, $e_1 = 7/8$ and $e_2 = 1/2$. Equation [2.15] yields a universal curve when plotted versus shape factor (Fig. 10).

The structure of scaling in Eq. [2.15] can be explained as follows. All curves in Eq. [2.15] converge as the shape factor approaches that of circle, $\tilde{G} = 1/4\pi \approx 0.08$. Hence, the middle factor in the first term on the right side of Eq. [2.15] compensates for the deviation of shape factor from that of a circle. The third

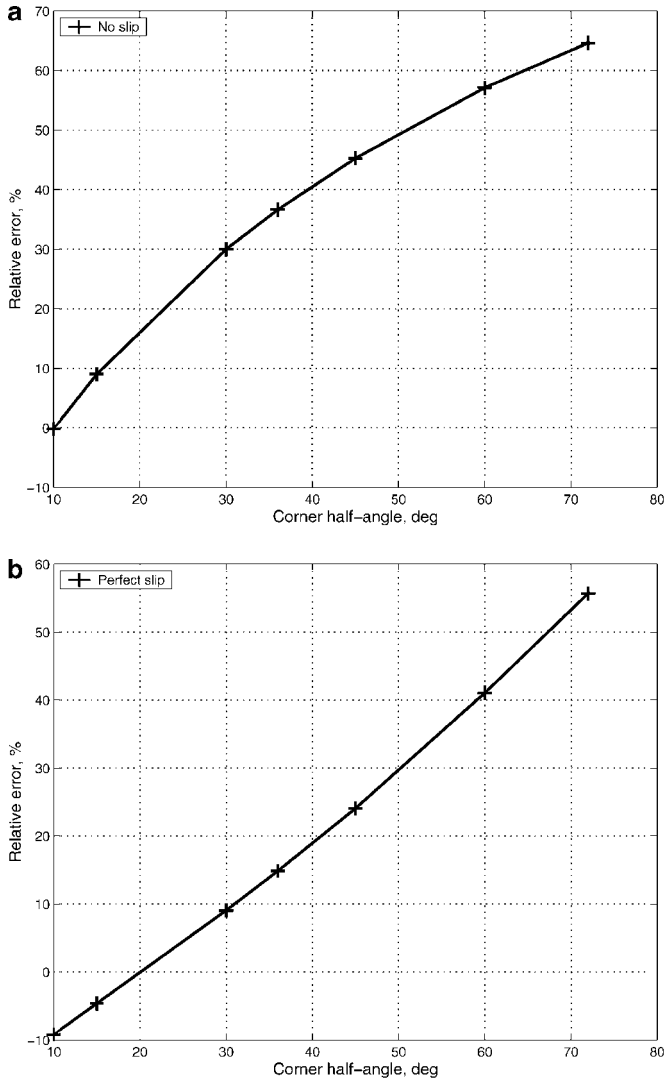


**FIG. 17.** Relative deviations of Zhou *et al.*'s analytical flow resistance factors from the corresponding FE solutions for zero contact angles: (a) no slip; (b) perfect slip.

factor in the first term in Eq. [2.15] compensates for the deviation of corner geometry from that of an equilateral triangle corner. In Eq. [2.15], the curves for the 45° and 15° corner half-angle are close to each other, as are those for the 60° and 10° corner half-angles. The last term on the right side of Eq. [2.15] moves the $\beta = 72^\circ$ corner half-angle points onto the universal curve.

For each corner half-angle, the scaling in Eq. [2.15] produces a slightly curving line. The respective lines nearly overlap and they can be approximated by a single quadratic function of the shape factor,

$$\tilde{g}_w = a_1\tilde{G}^2 + a_2\tilde{G} + a_3. \qquad [2.16]$$

The dimensional hydraulic conductance in corner flow is obtained by multiplying $\tilde{g}_w$ with the corresponding $b^4/\mu_w$.

The results of approximating the hydraulic conductances for each corner half-angle with the quadratic expressions [2.16] are shown in Fig. 11a and are listed in Table 3. The mean absolute error of these approximations is 1.02% (Fig. 12a). A single master-curve approximation is in turn compared with the finite element results in Fig. 12b. The mean absolute relative error of the latter approximation is 6.6%; however, for wide corner half-angles of 60° and 72°, and large contact angles, the relative error is 2–3 times larger (Fig. 12b).

### *4.2. Zero Surface Shear Viscosity*

Here we assume that no momentum is transferred across the interface, i.e., a perfect slip condition exists and the surface shear

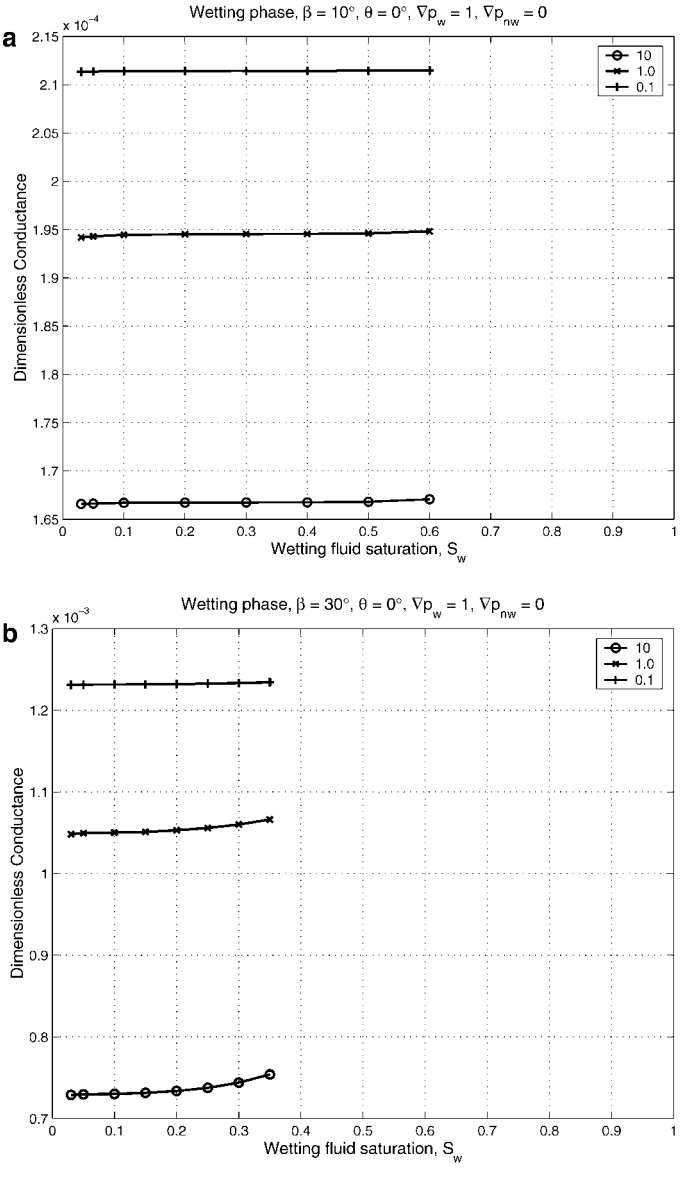


**FIG. 18.** The dimensionless hydraulic conductance in coupled flow of a perfectly wetting fluid as a function of the fluid saturation at three nonwetting–wetting fluid viscosity ratios. The corner half-angles are 10° (a) and 30° (b).

viscosity is zero. Correlation [2.15] holds, but the exponents are now $e_1 = 1$ and $e_2 = 0$. The calculated hydraulic conductances are listed in Table 4 and are shown in Fig. 13.

The quadratic approximations are listed in Table 5, plotted in Fig. 14, and compared with the finite-element calculations in Fig. 15. The mean absolute relative errors of the approximations are shown in Fig. 16. The quality of the approximations is not as good as in the no-slip case. The mean absolute error of individual approximations is 2.2%, while that of the master curve approximation is 15.9%. The main reason is that the correlation [2.15] does not collapse the sharp-corner conductances in the perfect-slip case as well as in the no-slip case.

### *4.3. Zhou et al. Analytical Expression for Resistance Factor*

Zhou *et al*. (3) presented an analytical solution for liquid flow along corners of angular capillaries and derived expressions for the flow resistance factors in two- and three-phase drainage with no-slip and perfect-slip conditions at the interfaces. Their results are compared in Fig. 17 with the corresponding finite element solutions at zero contact angle and for sharp corners. In two-phase flow, the mean absolute error of the Zhou *et al*. approximations is 35% in the no-slip case and 22% in the perfect-slip case. Thus, we find that in two-phase flow the scaling proposed here is superior to the expressions proposed by Zhou *et al*.

### *4.4. Shear Stress Continuity*

Finally, we consider the flow of two clean immiscible liquids and impose continuity of velocity and shear stress across the AM. First, we examine the hydraulic conductance of a perfectly wetting fluid as a function of its saturation and the ratio of the nonwetting to wetting fluid viscosity (Fig. 18). The wetting fluid is under the unit pressure gradient, and it drags the nonwetting fluid under the null pressure gradient. For the corner half-angle of 10°, the conductance is almost independent of saturation. As the viscosity ratio increases, the conductance decreases because of viscous drag exerted by the nonwetting fluid. For a wider corner half-angle of 30°, the conductance is higher and there is some dependence on saturation at the higher wetting fluid saturations. The universal correlation of hydraulic conductance for the continuous velocity case will be presented in a separate paper.

## 5. CONCLUSIONS

1. To calculate the hydraulic conductances of two immiscible Newtonian fluids, one preferentially wetting the solid surface, we have written a finite element program that describes the two-phase, creeping, isothermal flow in polygonal capillaries with no-slip, perfect-slip, and continuity of velocity and shear stress at the fluid interface. The program has been implemented in MATLAB®.

2. Our program automatically generates uniform Delaunay triangulations of the flow domains with the interface nodes that follow exactly the fluid interface. This property of our meshes makes the finite element solutions converge to the same degree of accuracy with about the same number of elements, regardless of the geometry of the corner and the meniscus, and regardless of the boundary condition at the interface. We have found that close to 6000 finite elements suffice to reach machine precision in two fluid-domain calculations.

3. We have tested thoroughly the convergence properties of our solutions and compared our wetting fluid conductances in sharp corners bound by concave menisci with the classical results of Ransohoff and Radke (2). We have found that their coarser-grid solutions differ from our converged solutions up to 4%.

4. The new results for the hydraulic conductances in corners bound by convex menisci with no-slip and perfect-slip boundary conditions have been listed.

5. With the velocity and stress continuity at the interface, the coupling coefficients are the same to within $10^{-14}$. The conductances of a perfectly wetting fluid dragging a nonwetting fluid have been plotted as functions of saturation, viscosity ratio, and corner geometry.

6. In two-phase flow in a polygonal capillary, the hydraulic conductance can be correlated with the corner filament shape factor, corner half-angle, and contact angle. The simple correlations proposed in this paper are very good for the no-slip boundary condition at the interface and reasonably good for the perfect-slip boundary condition.

7. Our correlations of hydraulic conductance of wetting liquid in two-phase flow are superior to those proposed by Zhou *et al*. (3).

8. Our correlations in corner flow bound by concave or convex menisci are simple and can be used in the computationally intensive large pore-network simulations of drainage and imbibition with contact line pinning and contact angle hysteresis.

## 6. APPENDIX: NOMENCLATURE

| | |
|---|---|
| $a$ | Equilateral triangle side, large half-axis of ellipse, m |
| $A$ | Cross-sectional area, $m^2$; small half-axis of ellipse, m |
| $b$ | Vertex–meniscus distance along pore wall, m |
| $e$ | Ellipse eccentricity |
| $E$ | Elliptic integral of second kind |
| $\vec{f}$ | Body force, N |
| $\tilde{g}_w$ | Scaled dimensionless conductance |
| $g$ | Hydraulic conductance, $m^4/N$ |
| G | Shape factor |
| $L$ | Pore length, m |
| $\vec{n}$ | Outward unit normal vector |
| $p$ | Pressure, Pa |
| $P$ | Perimeter, m |
| $Q$ | Volumetric flow rate, $m^3s^{-1}$ |
| $r$ | Inscribed circle radius, m |
| $\vec{v}$ | Fluid velocity, $ms^{-1}$ |
| $x_i$ | $i$th Cartesian axis, m |
| $\chi$ | Flow resistance factor |
| $\mu$ | Fluid viscosity, Pa-s |
| $\rho$ | Fluid density, $kgm^{-3}$ |
| $\beta$ | Tube corner half-angle, rad |
| $\Xi$ | Dimensionless negative pressure gradient |

| | |
|---|---|
| $\langle\ \rangle$ | Average quantity |
| $(\ )_w, (\ )_o$ | Wetting and nonwetting phase subscript |
| $\tilde{x}$ | Dimensionless quantity |

## ACKNOWLEDGMENTS

This work was supported in part by Otto Mønsteds Fond, Georg Schanargl Mindelegat, DONG, and U.C. Oil, Berkeley, through the contribution of Statoil. We would like to thank Dr. Paal-Eric Øren for sharing the numerical values of the hydraulic resistance factors calculated by Statoil.

## REFERENCES

1. Patzek, T. W., and Silin, D. B., *J. Colloid Interface Sci.* **236,** 295 (2001), doi: 10.1006/jcis.2000.7413.
2. Ransohoff, T. C., and Radke, C. J., *J. Colloid Interface Sci.* **121,** 392 (1987).
3. Zhou, D., Blunt, M., and Orr, F. M., Jr., *J. Colloid Interface Sci.* **187,** 11 (1997).
4. Dong, M., Dullien, F. A. L., and Chatzis, I., *J. Colloid Interface Sci.* **172,** 21 (1995).
5. Kwon, Y. W., and Bang, H., *in* "The Finite Element Method using MATLAB" (F. A. Kulacki, Ed.), CRC Mechanical Engineering Series. CRC Press, Boca Raton, FL, 1997.
6. Zienkiewicz, O. C., and Morgan, K., "Finite Elements and Approximation," Wiley, New York, 1983.
7. Kristensen, J. G., M.S. Thesis, Department of Materials Science & Mineral Engineering, U.C. Berkeley, Berkeley, CA, 1999.
8. Mathworks, I., "MATLAB—The Language of Technical Computing," MathWorks, Inc., Natick, MA, 1998.
9. Goode, P. A., and Ramakrishnan, T. S., *AIChE J.* **39**(7), 1124 (1993).